Maximum possible induced flow rates in open-ended vertical eccentric annuli with uniform heat flux

Esmail M.A. Mokheimer and Maged El-Shaarawi
Mechanical Engineering Department, King Fahd University of Petroleum and Minerals, Dhahran, Saudi Arabia

Received May 2003
Revised November 2003
Accepted December 2003

Abstract

Purpose – Obtaining the maximum possible flow rates that can be induced by free convection in open-ended vertical eccentric annuli under fundamental thermal boundary conditions of the fourth kind (heating or cooling one of the annulus walls with a uniform heat flux while keeping the other wall at ambient temperature). Obtaining the maximum possible flow rates that can be induced by free convection in open-ended vertical eccentric annuli under fundamental thermal boundary conditions of the fourth kind (heating or cooling one of the annulus walls with a uniform heat flux while keeping the other wall at ambient temperature).

Design/methodology/approach – The fully-developed laminar free convection momentum equation has been solved numerically using an analytical solution of the governing energy equation.

Findings – Results are presented to show the effect of the annulus radius ratio and the dimensionless eccentricity on the induced flow rate, the total heat absorbed by the fluid, and the fully developed Nusselt numbers on the two boundaries of the annulus for a fluid of Prandtl number 0.7.

Practical implications – Applications of the obtained results can be of value in the heat-exchanger industry, in cooling of underground electric cables, and in cooling small vertical electric motors and generators.

Originality/value – The paper presents a solution that is not available in the literature for the problem of fully developed free convection in open-ended vertical eccentric annular channels under thermal boundary conditions of the fourth kind. Also presents the maximum possible induced flow rates, the total heat absorbed by the fluid, and the Nusselt numbers on the two boundaries of the annulus. The effects of N and E (the radius ratio and eccentricity, respectively) on these results are presented. Such results are very much needed for design purposes of heat transfer equipment.

Keywords Flow, Convection, Channel flow

Paper type Research paper

Nomenclature

a = location of the positive pole of the bipolar coordinate system on the x-axis of the Cartesian coordinate system (constant in the bipolar transformation equations, equal to $r_i \sinh \eta_i$ or $r_o \sinh \eta_o$)

a^* = heat transfer coefficient, $q''/(T_w - T_m)$

A = cross-sectional area of the duct, $\pi (r_o^2 - r_i^2)$

A^* = constant of the integration in equation (10)

The authors gratefully acknowledge the support of King Fahd University of Petroleum and Minerals to carry out this work under Fast Track Project # FT/2003/10.

International Journal for Numerical Methods in Heat & Fluid Flow
Vol. 15 No. 2, 2005
pp. 161-182

0961-5539
DOI 10.1108/09615530510578438

A_i = inner surface area of the duct, $2\pi r_i l$

A_o = outer surface area of the duct, $2\pi r_o l$

B = constant of the integration in equation (10)

c_p = specific heat of the fluid at constant pressure

C = constant of the integration in equation (10)

D_h = hydraulic or equivalent diameter of annulus, $2(r_o - r_i) = 2a(1 - N)$ Csch η_o

D = constant of integration in equation (10)

e = eccentricity (distance between the axes of the two cylinders forming the eccentric annulus), $a(\coth \eta_o - \coth \eta_i)$

E = dimensionless eccentricity, $e/(r_o - r_i)$

f = volumetric flow rate,

$$f = \pi(r_o^2 - r_i^2)\bar{u} = 2\int_0^{\pi}\int_{\eta_o}^{\eta_i} uh^2 \, d\eta \, d\xi$$

F = dimensionless volumetric flow rate,

$$f/\pi l\gamma \mathrm{Gr}^* = 8(1 - N)^2 \times \int_0^{\pi}\int_{\eta_o}^{\eta_i} UH^2 \, d\eta \, d\xi/\pi$$

g = gravitational body force per unit mass(acceleration)

Gr = Grashof number, $\mp g\beta q D^4/2\gamma^2 k$ the plus and minus signs apply to upward (heating) and downward (cooling) flows, respectively. Thus, Gr is always positive

Gr* = modified Grashof number, $\mathrm{Gr}^* = \mathrm{Gr}\, D_h/l$

h = coordinate transformation scale factor, $a/(\cosh \eta - \cos \xi)$

H = dimensionless coordinate transformation scale factor,

$$h/D_h = \frac{0.5 \sinh(\eta_o)}{(1 - N)(\cosh(\eta) - \cos(\xi))}$$

i = index for the finite difference grid in η-direction

j = index for the finite difference grid in ξ-direction

k = thermal conductivity of fluid

l = height of the channel

m = number of intervals in ξ-direction

n = number of intervals in η-direction or infinite series summation index in the fully developed flow solution

N = radius ratio, $r_i/r_o = \sinh \eta_o/\sinh \eta_i$

$\mathrm{Nu}_y^{4.x}$ = local Nusselt number at any point on the inner or outer wall of the annulus where x and y are dummy variables; x represents the case under consideration which may be either I for an inner heated wall or O for an outer heated wall, while y stands for the specified wall and may also be either i or o for the inner and outer walls, respectively, $a^* D_h/k$

$\overline{\mathrm{Nu}_y^{4.x}}$ = Nusselt number averaged around the complete periphery of the y-wall of the annulus for a given Z where x and y are dummy variables explained above,

$$\frac{2(1 - N)}{N\pi}\int_0^{\pi} \mathrm{Nu}_i^{4.x} H(\eta_i, \xi) \, d\xi$$

on the inner wall or

$$\frac{2(1 - N)}{\pi}\int_0^{\pi} \mathrm{Nu}_o^{4.x} H(\eta_o, \xi) \, d\xi$$

on the outer wall

p = pressure at any cross-section

p_0 = pressure at annulus entrance

p_s = static pressure at elevation z, $-\rho_0 g z$

p' = pressure defect at any point, $p - p_s$

P = dimensionless pressure at any cross-section, $p' D_h^4/\rho_0 l^2 \gamma^2 \mathrm{Gr}^{*2}$

Pr = Prandtl number, $\mu\, c_p/k$

q'' = local heat flux at either boundary of the annulus defined to be positive when it heats the fluid, $-k\,\partial T/\partial n^* = \pm(k/h)(\partial T/\partial \eta)$ where the upper and lower signs stand for the inner and outer walls, respectively, in the case of fluid heating and vice versa in the case of fluid cooling

q = heat gained or lost by fluid from the entrance up to a particular elevation in the annulus, $\rho_0 f c_p(T_m - T_0)$

$\bar{q}$ = heat gained or lost by fluid from the entrance up to the annulus exit, i.e. value of q at $z = l$, $\rho_0 f c_p(\bar{T}_m - T_0)$

Q = dimensionless heat absorbed from the entrance up to any particular elevation, $q/[\pi\rho_0 c_p l\gamma \mathrm{Gr}^*(T_w - T_0)] = F\theta_m$

$\bar{Q}$ = dimensionless heat absorbed up to the annulus exit, i.e. value of Q at $z = l$, $\bar{q}/[\pi\rho_0 c_p l\gamma \mathrm{Gr}^*(T_w - T_0)] = F\bar{\theta}_m$

r_i = the radius of the inner cylinder of the annulus

r_o = the radius of the outer cylinder of the annulus

Ra = Rayleigh number, Gr Pr

Ra* = modified Rayleigh number, Gr* Pr = RaD_h/l

T = temperature at any point

T_m = mixing-cup (mixed-mean) temperature over any cross section of the annulus at a given z,

$$\int_A Tu\mathrm{d}A/(A\bar{u})$$

$$= 2\int_0^{\pi}\int_{\eta_o}^{\eta_i} Tu^2 \mathrm{d}\eta\mathrm{d}\xi/[\pi(r_o^2 - r_i^2)]$$

T_0 = ambient or entrance temperature

T_w = isothermal heated wall temperature

u = axial (streamwise) velocity component

$\bar{u}$ = average (mean) axial velocity,

$$\int_A u\mathrm{d}A/A$$

$$= 2\int_0^{\pi}\int_{\eta_o}^{\eta_i} uh^2 \mathrm{d}\eta\mathrm{d}\xi/[\pi(r_o^2 - r_i^2)]$$

$$= 2\int_0^{\pi}\int_{\eta_o}^{\eta_i} uh^2 \mathrm{d}\eta\mathrm{d}\xi/[\pi a^2(1-N^2)Csch^2\eta_o]$$

U = dimensionless axial velocity component, $ur_0^2/l\gamma \mathrm{Gr}^*$

X = the dimensionless first transverse direction in the Cartesian coordinate system, x/r_0

x = the first transverse direction in the Cartesian coordinate system

y = the second transverse direction in the Cartesian coordinate system

z = axial coordinate in both Cartesian and bipolar coordinate systems (measured from the annulus entrance)

Z = dimensionless axial coordinate in both Cartesian and bipolar coordinate systems, $z/(D_h\mathrm{Re})$

$$x = \frac{a\sinh(\eta)}{\cosh(\eta) - \cos(\xi)},$$

$$y = \frac{a\sin(\xi)}{\cosh(\eta) - \cos(\xi)}, z = z$$

Greek letters

α = thermal diffusivity of fluid, $k/\rho c_p$

η = the first transverse bipolar coordinate

η_i = value of η on the inner surface of the annulus,

$$\log_e\left[\frac{N(1+E^2)+(1-E^2)}{2NE} + \sqrt{\left(\frac{N(1+E^2)+(1-E^2)}{2NE}\right)^2 - 1}\right]$$

$$= \cosh^{-1}\left[\frac{N(1+E^2)+(1-E^2)}{2NE}\right]$$

η_o = value of η on the outer surface of the annulus,

$$\log_e\left[\frac{N(1-E^2)+(1+E^2)}{2E} + \sqrt{\left(\frac{N(1-E^2)+(1+E^2)}{2E}\right)^2 - 1}\right]$$

$$= \cosh^{-1}\left[\frac{N(1-E^2)+(1+E^2)}{2E}\right]$$

$\Delta\eta$ = numerical grid mesh size in η-direction, $(\eta_i - \eta_o)/n$

∇ = gradient operator

∇^2 = Laplacian operator

θ = dimensionless temperature, $\dfrac{T - T_0}{q'' D_h / k}$

μ = dynamic viscosity of fluid

γ = kinematic viscosity of fluid, μ/ρ

ξ = the second transverse bipolar coordinate

$\Delta\xi$ = numerical grid mesh size in ξ-direction, π/m

ρ = density of fluid

ϕ = normalized value of η, $(\eta - \eta_o)/(\eta_i - \eta_o)$

ψ = normalized value of ξ, ξ/π

Subscripts

c = circumferentially averaged

i = inner

iw = inner wall

o = outer

ow = outer wall

Introduction

Heat transfer in annuli occurs in the electrical field (Abdulhadi and Chato, 1977; Notaro and Webster, 1971), in the nuclear field (Lowry *et al.* 1980), and in petroleum engineering (Yonggang and Junfang, 1995). In the available literature, there are two essential papers dealing with fully developed laminar heat transfer in concentric annuli. The first of these, by Reynolds *et al.* (1963), presented for the first time a general formulation of the fully developed forced convection problem in concentric annuli for arbitrarily prescribed wall temperatures or heat fluxes. Four fundamental thermal boundary conditions were introduced. The second paper, by El-Shaarawi and Al-Nimr (1990), presented a detailed analysis and analytical solutions for the fully developed laminar free convection in vertical open-ended concentric annuli under the four fundamental thermal boundary conditions.

Fully developed forced convection in eccentric annuli can be found in Cladwell (1930), Piercy *et al.* (1933), Heyda (1959), Redberger and Charles (1962), Snyder (1963), Snyder and Goldstein (1965), Cheng and Hwang (1968), Trombeta (1972) and Guckes (1975)). In most of these papers, the governing momentum equation has been solved analytically using the solution given by El-Saden (1961) while, the governing energy equation has been solved numerically. While solving the developing flow problem, Feldman *et al.* (1982a, b) reported results for the fully developed forced convection in an eccentric annulus.

A thorough literature survey revealed that there are no solutions available for the problem of fully developed free convection in open-ended vertical eccentric annular channels other than those reported by the authors El-Shaarawi and Mokheimer (1999) and El-Shaarawi *et al.* (2001) for cases with isothermal boundary conditions of the first and third kinds. The lack of information regarding the fully developed free convection in open-ended vertical eccentric annuli with uniform heat flux conditions motivated the present work. This paper deals with free convection heat transfer in vertical eccentric annuli under fundamental thermal boundary conditions of the fourth kind. The paper presents the maximum possible induced flow rates, the total heat absorbed by the fluid, and the Nusselt numbers on the two boundaries of the annulus. The effects of N and E (the radius ratio and eccentricity, respectively) on the

results are presented. Such results are very much needed for design purposes of heat transfer equipment.

Problem formulation

As shown in Figure 1, the channel under consideration comprises an eccentric annulus of finite length, open at both ends and is vertically immersed in a stagnant Newtonian fluid of infinite extent maintained at constant temperature T_0. Free convection flow is induced inside this annular channel as a result of heating or cooling one of the channel walls with a uniform heat flux while keeping the other wall at ambient temperature. The uniform heat flux wall is called the active wall. If the active wall is the inner wall the case is referred to as case 4.I while case 4.O refers to the case in which the outer wall is the active wall. The fluid enters the channel at the ambient temperature T_0 and is assumed to have constant physical properties, but obeys the Boussinesq approximation according to which its density is allowed to vary with temperature in only the gravitational body force term of the vertical (axial) momentum equation. Body forces in other than the vertical direction, viscous dissipation, internal heat generation, and radiation heat transfer are absent. The latter assumption implies low emissivities of the annulus walls and low to moderate gap temperature differences.

The bipolar coordinates shown in Figure 2 are used to describe the problem. The relations between Cartesian and bipolar coordinates are given in the nomenclature.

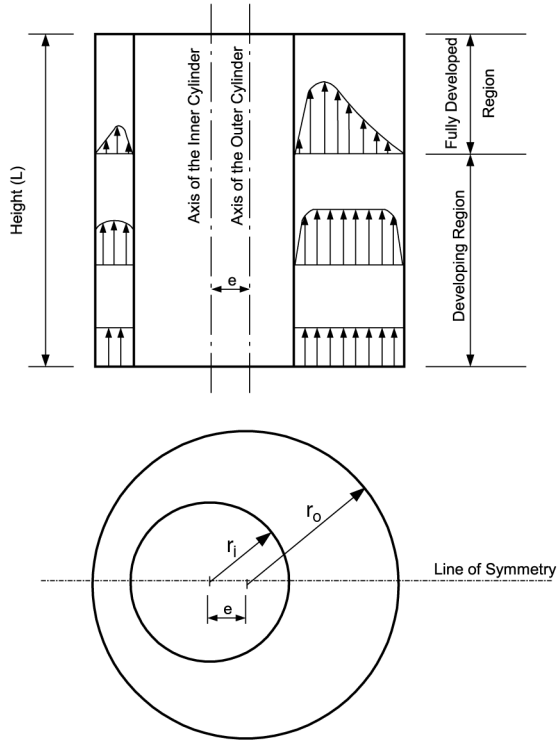

Figure 1.
Two-dimensional plane and elevation of the geometry under consideration

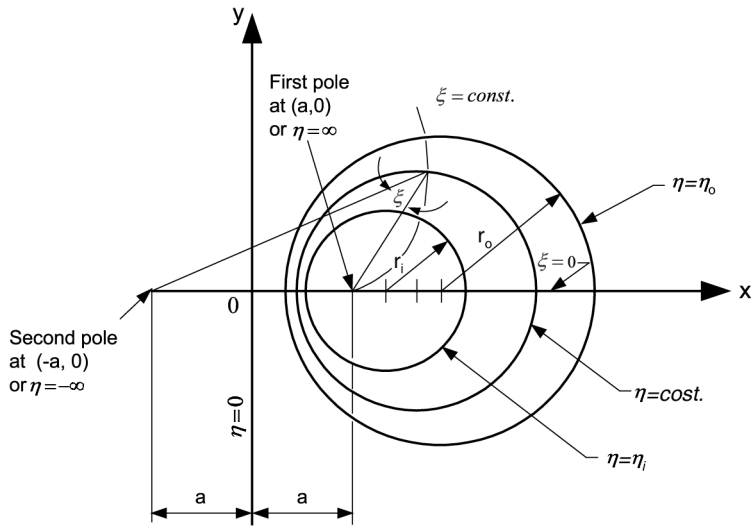

Figure 2.
Bipolar coordinate system

If the channel is sufficiently high, fully-developed free convection can be achieved. Fully developed flow conditions mean that the velocity components in η and ξ directions vanish, the axial velocity component u does not vary with the axial coordinate, i.e. $\partial u/\partial z = 0$ or $u = u(\eta, \xi)$, and the momentum and heat diffusion in the axial direction vanish, i.e. $\partial^2 u/\partial z^2 = \partial^2 T/\partial z^2 = 0$. Thus, the continuity equation automatically vanishes and the momentum equations in η and ξ directions reduce, respectively, to $\partial p/\partial \eta = 0$ (i.e. p is independent of η) and $\partial p/\partial \xi = 0$ (i.e. p is also independent of ξ). Consequently, the pressure is a function of z only (hence, $\partial p/\partial z = \mathrm{d}p/\mathrm{d}z$). Introducing the dimensionless parameters given in the nomenclature, the equations which govern the fully developed free convection in the present case become identical to those representing the case with isothermal boundary (El-Shaarawi *et al.*, 2001). These governing equations are the following coupled Z-momentum and energy equations, respectively.

$$\frac{1}{H^2}\left(\frac{\partial^2 U}{\partial \eta^2} + \frac{\partial^2 U}{\partial \xi^2}\right) - \frac{1}{4(1-N)^2}\,\frac{\mathrm{d}P}{\mathrm{d}Z} = -\frac{\theta}{4(1-N)^2} \tag{1}$$

$$\frac{1}{H^2}\left(\frac{\partial^2 \theta}{\partial \eta^2} + \frac{\partial^2 \theta}{\partial \xi^2}\right) = 4(1-N)^2 \,\mathrm{Pr}\, U\,\frac{\partial \theta}{\partial Z} \tag{2}$$

Owing to the presence of a plane of symmetry for the geometry under study, these two equations will be solved on one half of the annulus (i.e. $0 \le \xi \le \pi$) subject to the following hydrodynamic, thermal and symmetry conditions:

$$\left.\begin{array}{c}\text{For } \eta=\eta_{\mathrm{i}} \text{ or } \eta=\eta_{\mathrm{o}}, U=0 \\ \text{For } \xi=0 \text{ or } \xi=\pi,\ \partial U/\partial\xi=\partial\theta/\partial\xi=0 \\ \text{For Case 4.I}: \text{ at } \eta=\eta_{\mathrm{i}}, \left.\frac{\partial\theta}{\partial\eta}\right|_{\eta_{\mathrm{i}}}=\pm H(\eta_{\mathrm{i}},\xi) \text{ and at } \eta=\eta_{\mathrm{o}}, \theta=0 \\ \text{For Case 4.O}: \text{ at } \eta=\eta_{\mathrm{i}},\ \theta=0 \text{ and at } \eta=\eta_{\mathrm{o}} \left.\frac{\partial\theta}{\partial\eta}\right|_{\eta_{\mathrm{i}}}=\mp H(\eta_{\mathrm{o}},\xi)\end{array}\right\} \quad (3)$$

The plus and minus signs in the thermal boundary conditions on the inner wall ($\eta=\eta_{\mathrm{i}}$) are applicable for heating and cooling, respectively. However, the minus and plus signs in the thermal boundary conditions at ($\eta=\eta_{\mathrm{o}}$) are for heating and cooling, respectively.

Mathematical analysis

The mathematical analysis in this section is identical to that given by El-Shaarawi *et al.* (2001) and leads to the following equations.

$$\frac{\partial\theta}{\partial Z}=\frac{\mathrm{d}^2P}{\mathrm{d}Z^2} \quad (4)$$

$$\frac{1}{UH^2}\left(\frac{\partial^2}{\partial\eta^2}\left(\frac{1}{H^2}\left(\frac{\partial^2U}{\partial\eta^2}+\frac{\partial^2U}{\partial\xi^2}\right)\right)+\frac{\partial^2}{\partial\xi^2}\left(\frac{1}{H^2}\left(\frac{\partial^2U}{\partial\eta^2}+\frac{\partial^2U}{\partial\xi^2}\right)\right)\right)=\mathrm{Pr}\,\frac{\mathrm{d}^2P}{\mathrm{d}Z^2} \quad (5)$$

A solution of equation (5) in the form $U=U(\eta,\xi)$ is only possible if

$$\mathrm{d}^2P/\mathrm{d}Z^2=\alpha \quad (6)$$

where α is a constant. From equations (4) and (6), one can write

$$\partial\theta/\partial Z=\alpha \quad (7)$$

which means that, in the fully developed flow region, $\partial\theta/\partial Z$ is also constant and hence, for a point of given η and ξ, θ varies linearly with Z. Thus, regardless of the value of Pr, a hydrodynamically fully developed free convection $\partial\theta/\partial Z=0$ necessarily means that the flow has already been thermally fully developed.

In the cases under consideration (boundary conditions of fourth kind) at least one of the annulus boundaries (η_{i} or η_{o}) is kept isothermal and hence ($\partial\theta/\partial Z=0$) on such an isothermal boundary. The combination of equation (7) with an isothermal boundary condition leads to the conclusion that α, for such a fully-developed region, must equal zero ($\alpha=0$). Thus, the energy equation (2) reduces to the following:

$$\left(\frac{\partial^2\theta}{\partial\eta^2}+\frac{\partial^2\theta}{\partial\xi^2}\right)=0. \quad (8)$$

With $\alpha=0$, equation (6) means that the pressure gradient ($\mathrm{d}P/\mathrm{d}Z$) in the fully-developed region is constant (i.e. P varies linearly with Z). However, if the channel is extremely high the fully-developed region could occupy a very large portion of the channel height, the developing length could be neglected in comparison with that

of the fully-developed region and hence the assumption of fully-developed flow right from the channel entrance can be made. In this case, integrating equation (6) twice and applying the boundary conditions that the pressure is atmospheric at both inlet and exit of the annulus, i.e. $P = 0$ at $Z = 0$ and L (El-Shaarawi and Al-Nimr, 1990) leads to the following simplified form of equation (1).

$$\left(\frac{\partial^2 U}{\partial \eta^2} + \frac{\partial^2 U}{\partial \xi^2}\right) = -\frac{\theta}{4(1-N)^2} H^2 \tag{9}$$

Method of solution

The governing equations for the fully developed laminar free convection are equations (8) and (9) which are strongly coupled through the buoyancy term.

Analytical solution for the energy equation

The energy equation (8) subject to the aforesaid boundary conditions (3) can be solved analytically. A closed form analytical solution for this equation can be obtained as a special form of the general solution of the steady-state conduction problem given by El-Shaarawi and Mokheimer (1995) after neglecting the internal heat generation. In other words, the solution of equation (8) corresponds to the complementary part of the general solution given by El-Shaarawi and Mokheimer (1995) and can be written as:

$$\theta = A^* \eta + B + \sum_{n=1}^{\infty} (C e^{n\eta} + D e^{-n\eta}) \cos(n\xi) \tag{10}$$

where the values of the constants A^*, B, C and D are as follows:

	case 4.I	*case 4.O*
A^*	$\dfrac{0.5N}{1-N}$	$\dfrac{0.5}{1-N}$
B	$-A^* \eta_o$	$-A^* \eta_i$
C	$\dfrac{N}{n(e^{2n\eta_i} + e^{2n\eta_o})(1-N)}$	$\dfrac{1}{n(e^{2n\eta_i} + e^{2n\eta_o})(1-N)}$
D	$\dfrac{e^{2n\eta_o}}{n(e^{2n\eta_i} + e^{2n\eta_o})(1-N)}$	$\dfrac{e^{2n\eta_i}}{n(e^{2n\eta_i} + e^{2n\eta_o})(1-N)}$

Numerical solution for the momentum equation

The above analytical solutions for θ will be substituted in the momentum equation (9), which will then be solved numerically. Equation (9) can be replaced by the following finite-difference representation:

$$\frac{U(i-1,j)-2U(i,j)+U(i+1,j)}{(\Delta\eta)^2}+\frac{U(i,j-1)-2U(i,j)+U(i,j+1)}{(\Delta\xi)^2}$$

$$=\frac{-\theta(i,j)(H(i,j))^2}{4(1-N)^2}.$$

The above equation will be solved iteratively after rearranging its terms as follows:

$$U(i,j)=\frac{1}{2\left(\frac{1}{(\Delta\eta)^2}+\frac{1}{(\Delta\xi)^2}\right)}\left[\frac{U^*(i-1,j)+U^*(i+1,j)}{(\Delta\eta)^2}\right.$$
$$\left.+\frac{U^*(i,j-1)+U^*(i,j+1)}{(\Delta\xi)^2}+\frac{\theta(i,j)H^2(i,j)}{4(1-N)^2}\right] \quad (11)$$

in which i, j are indices for the numerical grid shown in Figure 3 and the asterisk in superscript means values from the previous iteration.

The problem under investigation is governed by three dimensionless parameters, namely, the radius ratio, N, the eccentricity, E, and the Prandtl number, Pr. For a fluid of a given Pr in an annulus of given N and E, the solution starts by calculating the corresponding values of η_i and η_o by means of the equations given in the nomenclature. Selecting the numbers of increments in η and ξ directions (n and m, respectively) the values of $\Delta\eta$ and $\Delta\xi$ can be computed.

The algorithm of solution is to assume a velocity field at all grid points, $U^*(i,j)$. Substitute these values of U^* together with the known values of $\theta(i,j)$ and $H(i,j)$ on the right hand side of equation (10) to obtain the new values of $U(i,j)$. If the relative error between U and U^* at all grid points $((U(i,j)-U^*(i,j))/U(i,j))$ satisfies a prescribed solution criterion ($\leq 10^{-4}$ per cent in the present work) the iteration process is stopped,

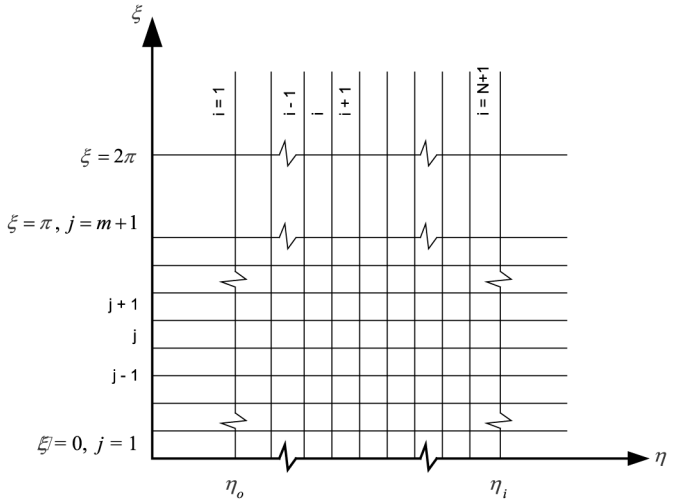

Figure 3.
The transformed geometry in η-ξ plane and the numerical mesh network

otherwise the iteration process continues after updating the values of U* according to the following relaxation equation:

$$U^*(i,j) = U^*_{\text{old}}(i,j) + w[U(i,j) - U^*_{\text{old}}(i,j)]. \tag{12}$$

In the above equation w is a relaxation factor which has been found to be 0.8 through numerical experimentation.

Having computed the local velocity values ($U(i,j)$), the average velocity can be expressed as a function of the local velocity by the equation:

$$\bar{U} = \frac{8}{\pi}\frac{1-N}{1+N}\int_0^{\pi}\int_{\eta_o}^{\eta_i} UH^2 \,\mathrm{d}\eta\,\mathrm{d}\xi. \tag{13}$$

The above integration has been evaluated numerically by the following representation:

$$\overline{\mathrm{U}} = \frac{8}{\pi}\frac{1-N}{1+N}\left(\sum_{j=2}^{m}\sum_{i=2}^{n} U(i,j)(H(i,j))^2 + 0.5\sum_{i=2}^{n}\left(U(i,1)(H(i,1))^2 + U(i,m+1)(H(i,m+1))^2\right)\right)\Delta\eta\,\Delta\xi \tag{14}$$

The induced flow rate is given by the following dimensional equation

$$f = 2\int_0^{\pi}\int_{\eta_o}^{\eta_i} uh^2 \,\mathrm{d}\eta\,\mathrm{d}\xi,$$

which in dimensionless form can be written as:

$$F = (1-N^2)\bar{U}. \tag{15}$$

Suitable mesh sizes in the η and ξ directions were chosen so that the numerical solution of the finite-difference equation is practically independent of the increment sizes in all directions. For example, the effect of the grid size on the results of the fully developed free convection in an eccentric annulus of radius ratio $N = 0.5$ and eccentricity $E = 0.5$ under the thermal boundary conditions 4.O has been investigated for different combinations of number of grid segments in the η and ξ directions. The investigated grid size ranged between 5×5 and 3×30 in the η and ξ directions. The impact of the grid size on the flow rate, heat absorbed and the average Nusselt numbers on the inner and the outer walls for the above mentioned case is given in Table I, taking the 30×30-grid results as the reference. This table shows that the maximum deviations between the results obtained via the 25×25 grid and that obtained via the 30×30 grid are about 0.14 per cent for the flow rate, 0.2 per cent for the heat absorbed, 0.05 per cent for the average Nusselt number at the inner wall and 0.28 per cent for the average Nusselt number at the outer wall. Thus, the 25×25 grid was adopted as it provides practically grid independent results and good compromise between the obtained accuracy and the computer CPU time.

The validity of the above method of solution and the developed computer code has been checked using an energy balance. This energy balance for the present fully

developed flow in an annulus with one wall kept isothermal implies that the heat crossing one wall should pass across the other wall. For both cases under consideration (4.I and 4.O) this energy balance means that, at any axial location (Z), the ratio of the average heat flux at the outer wall to that at the inner wall should always equal the radius ratio N. This has been checked and confirmed in all the computer runs and thus provided a means of validating the computer code and the accuracy of the algorithm used.

Comparing the results for the special case of concentric annuli with the corresponding closed-form solution of El-Shaarawi and Al-Nimr (1990) provided a second check on the validity of the present work. To simulate the concentric annuli using the present model and code, an infinitesimally small eccentricity, namely $E = 10^{-11}$, was chosen and special runs were conducted. This very low value of $E = 10^{-11}$ was used rather than the exact value of $E = 0.0$ because the latter cannot be used for computations in bipolar coordinates as it represents a singularity for transformation from the Cartesian to bipolar coordinates. Table II gives such a comparison for the induced flow rates over a wide range of the annulus radius ratio ($N = 0.1 - 0.9$) for both cases 4.I and 4.O. In this context, the authors would like to call the reader's attention to the following. The dimensionless temperature as defined

M × N	Flow rate, $F \times 10^3$	Difference (per cent)	Heat absorbed, $Q \times 10^3$	Difference (per cent)	Average Nusselt numer on the inner wall	Difference (per cent)	Average Nusselt number on the outer wall	Difference (per cent)
5 × 5	10.8362	10.669	64.6610	14.280	3.3517	4.213	6.792 1	17.171
10 × 10	11.8169	2.584	72.7626	3.540	3.2481	0.992	7.8094	4.766
15 × 15	12.0118	0.977	74.4197	1.343	3.2281	0.370	8.0486	1.849
20 × 20	12.0809	0.408	75.0092	0.561	3.2212	0.155	8.1362	0.780
25 × 25	12.1130	0.143	75.2838	0.197	3.2180	0.056	8.1775	0.277
25 × 30	12.1308	0.004	75.4365	0.005	3.2161	0.003	8.2007	0.006
30 × 25	12.1125	0.147	75.2800	0.202	3.2180	0.056	8.1767	0.287
30 × 30	12.1303	–	75.4327	–	3.2162	–	8.2002	–

Table I. Effect of grid size on the results of fully developed free convection, Case 4.O., $N = E = 0.5$, the reference values are those obtained using a 30 × 30 grid points mesh

The annulus radius ratio (N)	Case 4.I			Case 4.O		
	El-Shaarawi and Al-Nimr (1990) (Concentric)	Present work ($E = 10^{-11}$)	Difference (per cent)	El-Shaarawi and Al-Nimr (1990) (Concentric)	Present work ($E = 10^{-11}$)	Difference (per cent)
0.1	0.2209	0.2203	0.272	6.5379	6.4529	1.300
0.2	0.5055	0.5047	0.158	5.6417	5.5973	0.787
0.3	0.8943	0.8934	0.101	5.5282	5.4973	0.559
0.4	1.4404	1.4389	0.104	5.8047	5.7800	0.426
0.5	2.2367	2.2345	0.098	6.4423	6.4203	0.341
0.6	3.4693	3.4657	0.104	7.5778	7.5567	0.278
0.7	5.5722	5.5659	0.113	9.6220	9.5987	0.242
0.8	9.8472	9.8346	0.128	13.862	13.834	0.202
0.9	22.805	22.773	0.140	26.803	26.756	0.175

Table II. Validation of the present work with the closed form solution given by El-Shaarawi and Al-Nimr (1990) for the induced flow rate, $F \times 10^3$

by El-Shaarawi and Al-Nimr is twice that in the present article. Secondly, a thorough check of their closed form-solution for the flow rate in case 4.O revealed that it should be multiplied by a factor of 2 in order to be consistent with their definition of the dimensionless temperature. Thirdly, due to the different definitions of the dimensionless temperature in the two papers, the induced flow rates computed by the analytical solution of El-Shaarawi and Al-Nimr has to be divided by 2 in order to achieve consistency with the present definition and results.

The comparison given in Table II shows that the maximum deviation between the two flow-rate predictions is 0.27 per cent for case 4.I and 1.3 per cent for case 4.O. Thus, there is excellent agreement between the values of the induced flow rates predicted via the present model and code with those predicated via the analytical solution of El-Shaarawi and Al-Nimr (1990).

Results and discussions

Induced flow results

Figure 4(a) shows, for a slight eccentric annulus ($E = 0.1$), the obtained fully developed velocity profiles corresponding to cases 4.I and 4.O, as one rotates around the annulus from its widest gap side ($\psi = \xi/\pi = 0$) to its narrowest gap side ($\psi = 1$, i.e. $\xi = \pi$). To have an insight into the effect of the eccentricity on the velocity profiles, Figure 4(b) shows the obtained fully developed velocity profiles in the widest and narrowest sides of the annulus for cases 4.I and 4.O with two values of eccentricity, namely $E = 0.1$ and 0.5. As can be seen from Figure 4(a) and (b) in either case 4.I or 4.O, the heating of a boundary causes the velocity profiles to be skewed towards this boundary (i.e. shifts the point of maximum velocity towards the heated boundary, thus the maximum velocity point becomes remarkably closer to the inner wall in case 4.I). Moreover, these figures also show that, for a given E, the velocity profile has larger values in case 4.O than in case 4.I. Thus, larger induced volumetric flow rates are

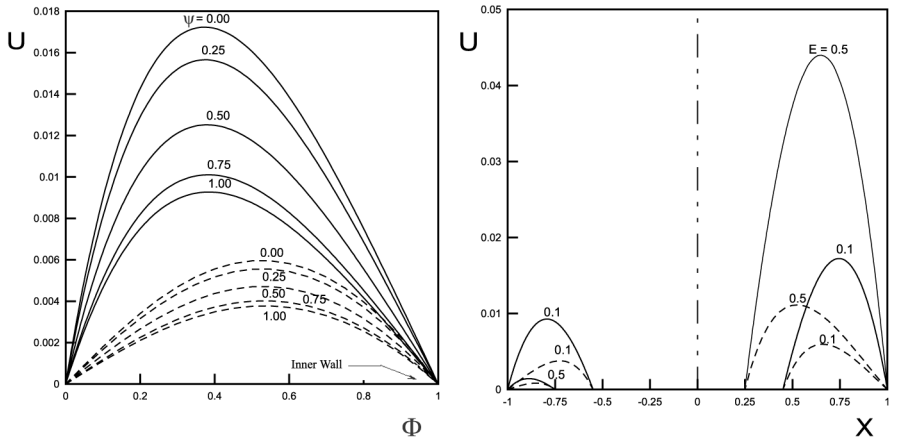

(a) Effect of the thermal boundary conditions on the velocity profile through the annulus form ψ = 0.0 to ψ = 1.0, - - - - - Case 4.I, ——— Case 4.O

(b) Effect of eccentricity on the velocity profile for radius ratio N = 0.5, - - - - - Case 4.I, ——— Case 4.O

Figure 4.
Effect of the thermal boundary conditions and eccentricity

anticipated in case 4.O. This is attributed to the larger heating surface area in case 4.O when compared with case 4.I.

Figure 4(b) shows the effect of the eccentricity on the velocity profile; asymmetry increases with E. The phenomenon of the asymmetric axial-velocity profiles is attributed to the increase/decrease in the resistance to flow in the narrow/wide side of the annular gap as a result of eccentricity. The resistance to flow in the narrowest gap will always be larger than that in the widest gap because of higher velocity gradients in the former than the latter. Thus, increasing the eccentricity (E) increases/decreases the values of U in the widest/narrowest side of the gap. However, a net result will be an increase in the average value $\overline{U}$ and consequently, F as will be shown later for both cases 4.I and 4.O for all values of radius ratio N, except for case 4.I. with small radius ratio.

Engineers are usually interested in the induced flow rate (F) rather than the above details of the velocity profiles. For given N and E, this flow rate (F), that is obtained from the fully-developed velocity profile, is the maximum possible that a vertical eccentric annulus can engender under the free convection thermal boundary conditions of the fourth kind. In other words, since fully developed flow conditions have already been achieved, a further increase in the channel height would not produce any additional flow. For a given annulus, a flow rate higher than this maximum possible value can be achieved only by forced convection. Table III gives values of F over wide ranges of N and E. As shown in Table III, for a given E, the dimensionless induced flow rate F increases with N for both cases 4.I and 4.O. On the other hand, for a given N, the flow rate F generally increases with E except for case 4.I with small eccentricity and radius ratio. Moreover, the flow rate in case 4.O is larger, for given N and E, than the corresponding value in case 4.I. This is a result of the larger heating surface in the former case than the latter.

Heat transfer results

To clarify the effect of eccentricity on the temperature distribution, the variation of the temperature around the active wall, in an annulus having $N = 0.5$, has been plotted in Figure 5(a) and (b) for cases 4.I and 4.O, respectively. These figures show that the temperature around the active wall is not uniform. This is because the fluid thermal resistance decreases as one rotates around the annulus from its widest side ($\psi = \xi / \pi = 0$) to its narrowest side ($\psi = 1$) since the thickness of the fluid layer decreases in the same direction. Figure 5(a) and (b) also shows that the non-uniformity of the temperature around the active wall increases with increase in eccentricity for both cases 4.I and 4.O.

The circumferentially averaged temperature on the active wall has been computed using the numerical representations for the following two equations on the inner and outer walls, respectively.

$$\overline{(\theta_{\mathrm{iw}})_c} = \frac{2(1-N)}{N\pi}\int_0^{\pi} \theta(\eta_{\mathrm{i}}, \xi)H(\eta_{\mathrm{i}}, \xi)\mathrm{d}\xi \tag{16}$$

$$\overline{(\theta_{\mathrm{ow}})_c} = \frac{2(1-N)}{\pi}\int_0^{\pi} \theta(\eta_{\mathrm{o}}, \xi)H(\eta_{\mathrm{o}}, \xi)d\xi \tag{17}$$

Figure 6(a) shows that for a given N, the circumferentially averaged temperature on the inner heated wall decreases in case 4.I with eccentricity. This is attributed to the

Table III.
The maximum possible induced flow rate and heat absorbed by free convection in eccentric annuli under thermal boundary conditions 4.I. and 4.O

	N																	
	0.1		0.2		0.3		0.4		0.5		0.6		0.7		0.8		0.9	
E	4.I	4.O	4.I	4.O	4.I	4.O	4.I	4.O	4.I	4.O	4.I	4.O	4.I	4.O	4.I	4.O	4.I	4.O
Case																		
Flow rate, $F\times10^3$																		
0.1	0.220	6.585	0.506	5.748	0.900	5.667	1.457	5.973	2.271	6.641	3.536	7.817	5.697	9.924	10.09	14.29	23.42	27.60
0.2	0.217	6.982	0.509	6.202	0.919	6.180	1.508	6.552	2.380	7.306	3.745	8.603	6.087	10.91	10.86	15.66	25.35	30.14
0.3	0.213	7.642	0.513	6.963	0.950	7.041	1.591	7.527	2.559	8.426	4.089	9.928	6.735	12.56	12.15	17.98	28.61	34.44
0.4	0.207	8.562	0.517	8.036	0.988	8.259	1.703	8.911	2.801	10.02	4.565	11.82	7.639	14.93	13.96	21.29	33.21	40.56
0.5	0.197	9.741	0.518	9.430	1.031	9.850	1.835	10.72	3.102	12.11	5.164	14.31	8.794	18.05	16.30	25.65	39.21	48.61
0.6	0.183	11.17	0.514	11.16	1.075	11.83	1.984	12.99	3.451	14.74	5.878	17.44	10.20	21.99	19.18	31.15	46.66	58.73
0.7	0.164	12.86	0.503	13.25	1.113	14.24	2.142	15.75	3.940	17.94	6.697	21.27	11.84	26.81	22.60	37.88	55.64	71.10
0.8	0.139	14.77	0.482	15.75	1.143	17.09	2.300	19.03	4.258	21.77	7.611	25.86	13.72	32.60	26.59	45.96	66.23	85.89
0.9	0.109	16.90	0.449	18.65	1.158	20.46	2.451	22.90	4.696	26.29	8.611	31.29	15.83	39.46	31.16	55.53	78.53	103.36
Heat absorbed, $\bar{Q}\times10^5$																		
0.1	0.792	645.8	3.490	415.7	8.969	333.5	18.70	299.2	35.33	290.8	64.09	304.7	117.1	348.7	230.9	457.4	587.2	811.1
0.2	0.762	712.3	3.437	473.2	9.047	387.1	19.33	351.1	37.37	342.8	69.22	359.0	128.9	409.3	258.2	533.2	665.5	937.9
0.3	0.713	825.7	3.344	572.2	9.155	479.7	20.31	441.1	40.65	433.1	77.66	453.5	148.5	514.5	304.2	664.7	798.8	1157
0.4	0.646	990.4	3.206	717.8	9.261	616.6	21.57	574.4	45.03	567.3	89.22	593.9	176.0	670.8	369.8	859.4	991.2	1479
0.5	0.562	1213	3.017	918.0	9.327	805.5	22.99	758.6	50.31	752.8	103.7	788.3	211.2	887.0	455.9	1128	1249	1920
0.6	0.466	1505	2.774	1184	9.310	1057	24.45	1004	56.25	1000	120.7	1048	254.2	1175	563.9	1484	1579	2500
0.7	0.360	1882	2.476	1534	9.167	1386	25.82	1323	62.59	1322	140.0	1385	304.9	1549	695.3	1945	1990	3246
0.8	0.253	2370	2.128	1990	8.865	1810	26.96	1734	69.07	1734	161.2	1816	363.3	2027	851.9	2532	2493	4186
0.9	0.154	3016	1.744	2592	8.383	2357	27.77	2257	75.45	2257	184.0	2362	429.5	2630	1036	3268	3099	5358

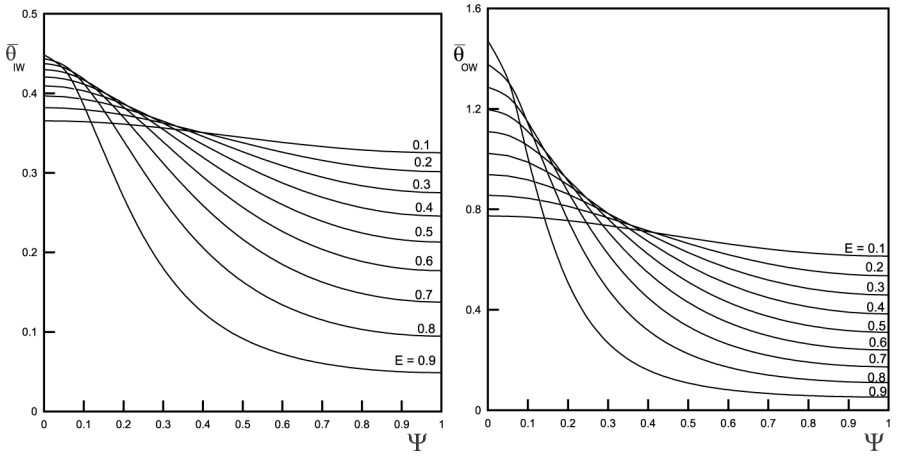

(a) Effect of eccentricity on the temperature variation around the inner wall for Case 4.I, N = 0.5

(b) Effect of eccentricity on the temperature variation around the outer wall for Case 4.O, N = 0.5

Figure 5.
Effects of eccentricity on temperature variation

increase in the induced flow rate that occurs with the increase in the value of E. Consequently, the boundary layers developed on both boundaries of the annulus become thinner as E increases and the resistances to the heat transfer decrease. Since the cooling effect on the outer wall is more dominant than the heating effect on the inner wall (since A_o is greater than A_i), the temperature level on the inner wall decreases with eccentricity.

On the other hand, Figure 6(b) shows that for a given N, the circumferentially averaged temperature on the outer heated wall increases in case 4.O with E. Again this is

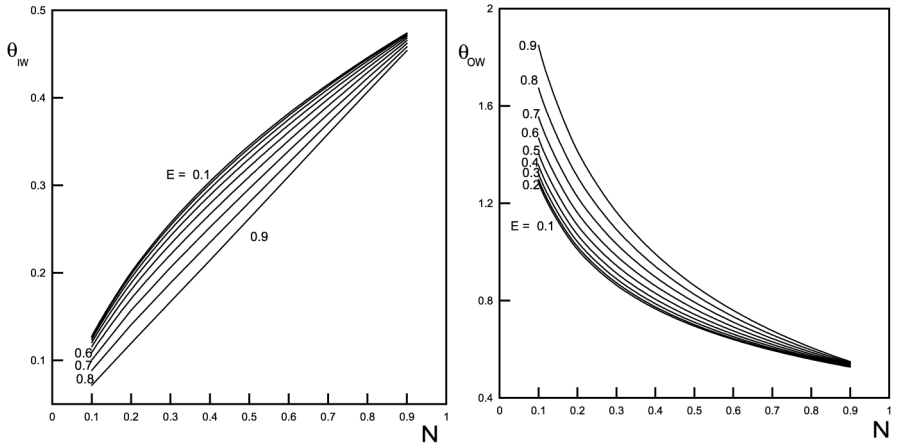

(a) Effect of eccentricity on the circumferentially averaged temperature at the inner wall against radius ratio for Case 4.I

(b) Effect of eccentricity on the circumferentially averaged temperature at the outer wall against radius ratio for Case 4.O

Figure 6.
Effects of eccentricity on circumferentially averaged temperature

attributed to the decrease in thermal resistance on the two walls. However, in case 4.O, the cooling on the inner wall is not dominant as it is on the outer wall in case 4.I and consequently, the temperature on the outer wall increases with E.

The bulk fluid temperature can be calculated as follows:

$$T_m = \frac{\int_A Tu \, \mathrm{d}A}{f} = \frac{\int_X \int_Y Tu \, \mathrm{d}x \, \mathrm{d}y}{f} \tag{18}$$

which in a dimensionless form is

$$\theta_m = \frac{8}{\pi} \frac{1-N}{1+N} \frac{\int_0^{\pi} \int_{\eta_o}^{\eta_i} \theta U H^2 \mathrm{d}\eta \, \mathrm{d}\xi}{\overline{U}}. \tag{19}$$

This integration has been evaluated numerically and computed by the following equation.

$$\theta_m = \frac{8}{\pi} \frac{(1-N)}{(1+N)\overline{U}} \left(\begin{array}{l} \sum_{j=2}^{m} \sum_{i=2}^{n} \theta(i,j) U(i,j) (H(i,j))^2 \\ +0.5 \sum_{i=2}^{n} \left(\begin{array}{l} \theta(i,1) U(i,1) (H(i,1))^2 \\ +\theta(i,m+1) U(i,m+1) (H(i,m+1))^2 \end{array} \right) \end{array} \right) \Delta\eta \Delta\xi \tag{20}$$

The variations of the bulk fluid temperature with N and E are shown in Figure 7(a) and (b) for cases 4.I and 4.O, respectively. These two figures show that, for a given E, the

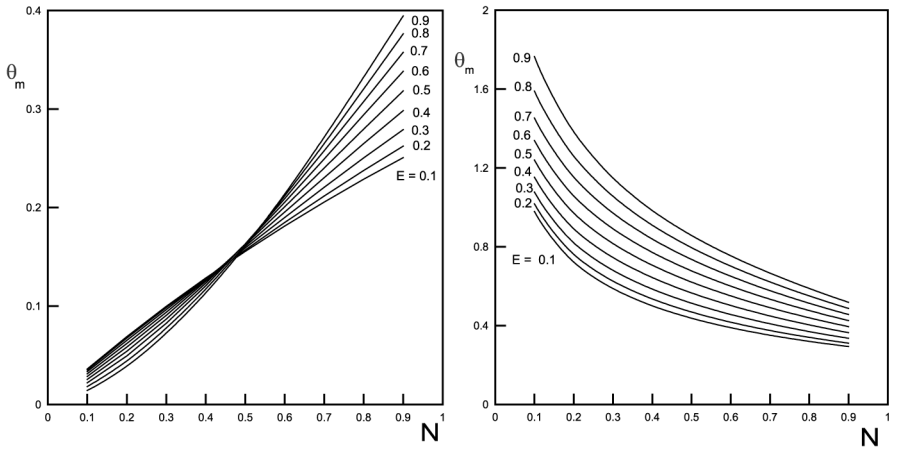

(a) Effect of eccentricity on the mean bulk temperature against the radius ratio for Case 4.I,

(b) Effect of eccentricity on the mean bulk temperature against the radius ratio for Case 4.O

Figure 7.
Effect of eccentricity on mean bulk temperature

increase in the radius ratio leads to an increase in the mean bulk temperature for case 4.I and vice versa for case 4.O. This can be explained by taking into consideration that the ratio of the inner surface area (A_i) to the outer surface area (A_o) equals the radius ratio (N). Thus, increasing N means that the ratio of the inner heating surface area to the outer cooling surface area in case 4.I increases and consequently, θ_m increases with N. On the other hand, in case 4.O, the increase in the value of N means an increase of the ratio of the inner cooling surface area to the outer heating surface area and hence θ_m decreases with N.

For case 4.O, the mean (bulk) fluid temperature, for a given N, increases with eccentricity, as seen in Figure 7(b). This is due to the simultaneous increase in F and the circumferentially averaged heated outer wall temperature ($\overline{\theta_{ow}}$), which have been explained before. On the other hand, the variation of θ_m with E for a given N in case 4.I (Figure 7(a)) can be attributed to the contradicting effects of E on F and $\overline{\theta_{iw}}$ (circumferentially averaged heated inner wall temperature), which have been explained before. However, for large radius ratios ($N > 0.5$) the mean bulk temperature increases with the radius ratio N. This is attributed to the increase in the heating surface area at the inner wall with respect to the cooling surface area at the outer wall. Increasing the radius ratio makes the heating/cooling surface area at the inner/outer wall approach each other and the cooling effect of the outer wall becomes less dominant and the bulk fluid temperature increases with E.

The local Nusselt number has been calculated based on the local dimensionless heat flux on the boundaries and the final derived formulas are as follows.

Case	*Inner wall*	*Outer wall*
4.I	$\mathrm{Nu}_i^{4.I} = \dfrac{1}{\theta_{iw} - \theta_m}$	$\mathrm{Nu}_o^{4.I} = \dfrac{1}{\theta_m}\left(\dfrac{1}{H}\dfrac{\partial\theta}{\partial\eta}\right)\Big\vert_{\eta_o}$
4.O	$\mathrm{Nu}_i^{4.O} = -\dfrac{1}{\theta_m}\left(\dfrac{1}{H}\dfrac{\partial\theta}{\partial\eta}\right)\Big\vert_{\eta_i}$	$\mathrm{Nu}_o^{4.O} = \dfrac{1}{\theta_{ow} - \theta_m}$

The circumferential variations of the local Nusselt number on the inner and outer walls of the annulus have been calculated for cases 4.I and 4.O. Unpresented results show that, in general, the local Nusselt number on the active wall is larger than that on the isothermal wall. For the isothermal wall (either the outer wall in case 4.I or the inner wall in case 4.O) the circumferentially averaged Nusselt number has been computed by integrating the local Nusselt number around the pertinent wall, using the following two equations:

$$\text{Case 4.I}: \quad \overline{\mathrm{Nu}_o^{4.I}} = \frac{2(1-N)}{\pi}\int_0^{\pi}\left(\mathrm{Nu}_o^{4.I}\right)H(\eta_o, \xi)\,d\xi = \frac{N}{\theta_m} \tag{21}$$

$$\text{Case 4.O}: \quad \overline{\mathrm{Nu}_i^{4.O}} = \frac{2(1-N)}{N\pi}\int_0^{\pi}\left(\mathrm{Nu}_i^{4.O}\right)H(\eta_i, \xi)\,d\xi = \frac{1}{N\theta_m} \tag{22}$$

For the uniform heat flux wall, the following equations have been used to compute the circumferentially averaged Nusselt number:

$$\text{Case 4.I:}\quad \overline{\mathrm{Nu}_{\mathrm{i}}^{4.\mathrm{I}}} = \frac{1}{(\overline{\theta_{\mathrm{iw}}})_{\mathrm{c}} - \theta_m} \tag{23}$$

$$\text{Case 4.O:}\quad \overline{\mathrm{Nu}_{\mathrm{o}}^{4.\mathrm{O}}} = \frac{1}{(\overline{\theta_{\mathrm{ow}}})_{\mathrm{c}} - \theta_m} \tag{24}$$

Formulae (23) and (24) are based on the energy balance used by Trombeta (1972). This energy balance uses the temperature difference between the circumferential averaged wall temperature on the active wall and the fluid mean bulk temperature rather than the local temperature difference in the calculations of the heat transfer coefficient (Nusselt number). The variations of the circumferentially averaged Nusselt number on the inner and outer walls with the radius ratio N for different values of the eccentricity (E) are plotted in Figures 8(a) and (b) and 9(c) and (d) for cases 4.I and 4.O, respectively. These figures show that the circumferentially averaged Nusselt number on the active wall is in general larger than that on the isothermal wall. However, in case 4.O with small radius ratio and small eccentricity, the opposite is true. This behaviour of the circumferentially averaged Nusselt number on both the inner and outer walls of the annulus is explained hereafter.

In isothermal annular flows, the hydrodynamic boundary layer on the inner boundary is thinner than that on the outer boundary. However, the heat transfer makes the flow faster/slower near the active/isothermal wall of the annulus. Hence, in case 4.I (in which the active wall is the inner wall), the heat transfer and the nature of the annular flow work together to make the hydrodynamic boundary-layer on the inner wall much thinner than that on the outer wall, resulting in larger values of Nusselt number on the inner wall compared to that on the outer wall. In case 4.O (in which the outer wall is the active wall), the heat transfer effect opposes the annular flow requirements as it makes the flow faster/slower near the outer/inner wall of the

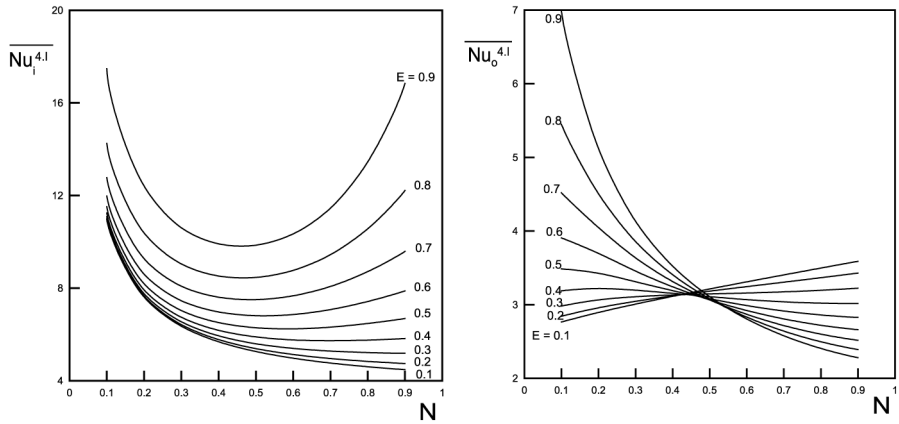

(a) Effect of eccentricity on the circumferentially averaged Nusselt number on the inner active wall against the radius ratio for Case 4.I

(b) Effect of eccentricity on the circumferentially averaged Nusselt number on the isothermal outer wall against the radius ratio for Case 4.I

Figure 8.
Effect of eccentricity on circumferentially averaged Nusselt number (case 4.I)

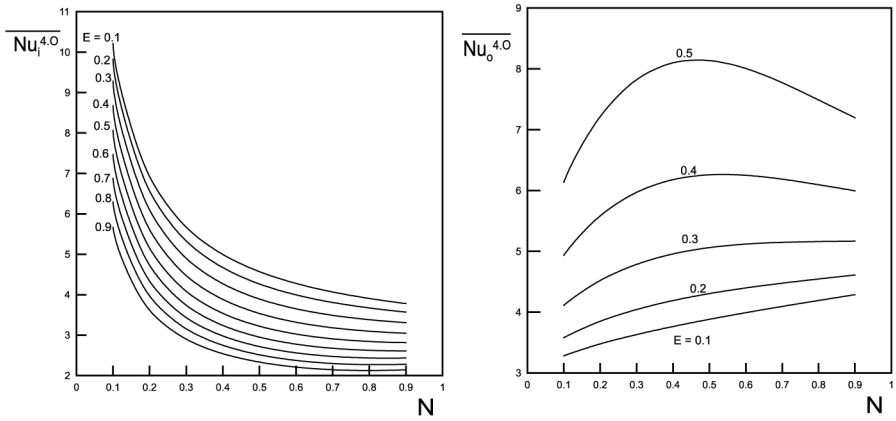

(a) Effect of eccentricity on the circumferentially averaged Nusselt number on the inner isothermal wall against the radius ratio for Case 4.O

(b) Effect of eccentricity on the circumferentially averaged Nusselt number on the outer active wall against the radius ratio for Case 4.O (E = 0.1-0.5)

Figure 9.
Effect of eccentricity on the circumferentially averaged Nusselt number (Case 4.O)

annulus (i.e. thickening the hydrodynamic boundary layer developed on the inner wall). For low eccentricities the effect of the annular flow feature overcomes that of the heat transfer and the circumferentially averaged Nusselt number is larger on the inner isothermal wall than that on the outer active wall. However, for larger eccentricities the heat transfer effect becomes dominant and the circumferentially averaged Nusselt number is larger on the outer active wall than that on the inner isothermal wall.

Figure 8(a) shows that the Nusselt number at the inner heated wall for case 4.I decreases with the radius ratio for small eccentricities ($0.1 \leq E \leq 0.4$). However, for larger eccentricities ($E \geq 0.5$) the Nusselt number decreases with radius ratio till it reaches a minimum value at radius ratio equal to 0.5 approximately, then it increases with the radius ratio. This can be attributed to the effect of each of N and E on θ_m and F. As shown in Figure 7(a), θ_m increases with N for all values of E. The increase in the value of θ_m will reduce the heat transfer from the active wall (inner wall in this case) to the fluid, i.e. a reduction in the value of $Nu_i^{4.I}$ with N. However, increasing E increases the flow rate F and consequently, increases the heat transfer (due to thinning of the boundary-layers on the walls). Thus, for large values of E ($E > 0.5$) the increase in the heat transfer (due to the increase in F) overcompensates the reduction in heat transfer (due to the increase in N) and the behaviours of $Nu_i^{4.I}$ with N and E shown in Figure 8(a) are obtained. In other words, there is a continuous decrease in the circumferentially averaged Nusselt number on the inner heated wall with the increase in the radius ratio (N) for low range of eccentricity $E < 0.5$. However, for $E > 0.5$, Nusselt number on the inner wall decreases with N to its minimum value at about $N \approx 0.5$, then it increases with N.

Figure 8(b) shows the circumferentially-averaged Nusselt number on the outer wall in case 4.I against the radius ratio N for various values of the parameter E. For low range of radius ratio ($N < 0.5$), the Nusselt number on the outer wall increases with eccentricity. This can be attributed to the decrease in the bulk temperature with the

eccentricity for the low range of radius ratios ($N < 0.5$) as shown in Figure 7(a) and consequently, an increase in Nusselt number with E according to equation (21). For high values of eccentricity ($E > 0.5$), the bulk temperature increases with N, as shown in Figure 7(a), and this results in a decrease in Nusselt number with N according to equation (21).

For case 4.O, the variation of the circumferentially-averaged Nusselt number on the inner isothermal wall against the radius ratio N is shown in Figure 9(a) for various values of E. This behaviour can be directly explained by the mathematical expression of the circumferentially averaged Nusselt number as function of N and θ_m(equation (22)). This equation shows that the circumferentially averaged Nusselt at the isothermal inner wall is inversely proportional to N and θ_m. For a given value of eccentricity, θ_m decreases with N as shown in Figure 7(b). Thus, increasing the radius ratio N, for case 4.O, results in a decrease in the circumferentially-averaged Nusselt number for any value of E. Similarly, for a given N, the fluid bulk temperature increases with the eccentricity E, which leads to a direct decrease in the circumferentially averaged Nusselt number with E.

Figures 9(a) and 10(a) and (b) show the variation of the circumferentially averaged Nusselt number with N as computed by equation (24) for different eccentricities. Physically this behaviour can be attributed to the fact that the annular flow features make the boundary layer thick at the outer wall. However, this annular flow feature, in case 4.O, is opposed by the heating effect at this wall, which causes thinning of the boundary layer at this wall. The effect of the flow features on the thickness of the boundary layer at the outer heated wall decreases with the eccentricity (as F increases with E). For large value of eccentricity ($E > 0.3$), Nusselt number at the outer heated wall increases with N reaching a maximum value at $N \cong 0.5$. Increasing the radius ratio above $N = 0.5$ makes the cooling effects at the inner wall more significant due to

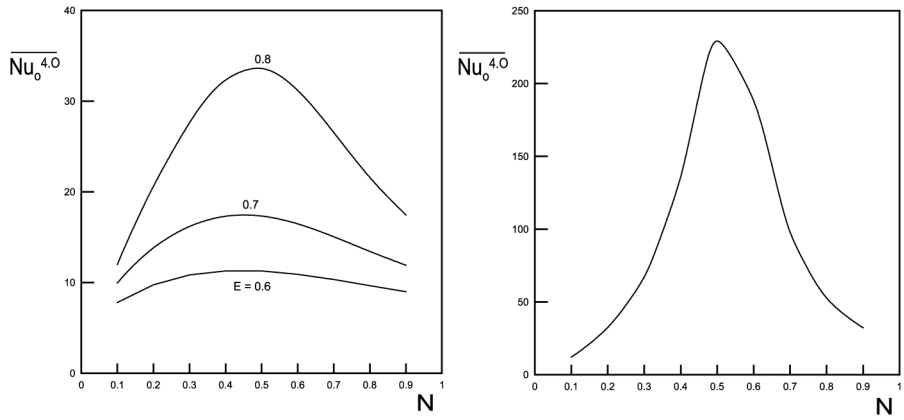

(a) Effect of eccentricity on the circumferentially averaged Nusselt number on the inner isothermal wall against the radius ratio for Case 4.O (E = 0.6-0.8)

(b) Effect of radius ratio on the circumferentially averaged Nusselt number on the outer active wall for Case 4.O for E = 0.9)

Figure 10.
Effect of eccentricity on the circumferentially averaged Nusselt number

the increase in the cooling surface area of the inner wall, resulting in a decrease in θ_m which leads to a decrease in Nusselt number with N from its maximum value attained at $N \cong 0.5$ for all values of $E > 0.3$.

Engineers are interested in the induced flow rate and the maximum (in case of heating) or minimum (in case of cooling) bulk temperature that the fluid attains as it passes through the channel and reaches its exit cross-section ($\bar{T}_m$). The latter can be used to calculate the heat gained or lost by the fluid from entrance up to the annulus exit ($\bar{Q}$). This latter important engineering parameter ($\bar{Q}$) can be used directly instead of using the Nusselt numbers on both walls. Therefore, it is given in Table III. From this table we see that the the flow rate F and the heat absorbed $\bar{Q}$ in case 4.O are larger, for a given N and E, than the corresponding values in case 4.I. This is a result of the larger heating surface in the former case than the latter.

Under thermal conditions of the fourth kind, the fully developed θ and hence θ_m do not vary with axial distance (Z). The bulk temperature θ_m does not change with further increase in the channel height since, under fully-developed flow conditions, the heat passes through the fluid from one wall is lost through the other wall. Thus, for a given N and E, the computed fully-developed value of θ_m corresponds also to the fluid bulk temperature at the channel exit $\bar{\theta}_m$ (i.e. $\theta_m = \bar{\theta}_m$). The computed values of $\bar{\theta}_m$ and F are used to obtain $\overline{Q}$ ($= F\bar{\theta}_m$) which is presented in Table III. Thus, the total heat gained or lost by the fluid from entrance up to the channel exit, including the neglected developing length, is obtained without need to integrate the Nusselt number over the channel height.

Conclusion

Fully developed laminar free convection in vertical open-ended eccentric annuli has been investigated for thermal boundary conditions of the fourth kind. The governing momentum equation has been solved numerically using an analytical solution for the governing energy equation. Numerical results have been obtained for a fluid of Prandtl number 0.7 in annuli of various radius ratios ($N = 0.1 - 0.9$) over a wide range of the dimensionless eccentricity ($E = 0.1 - 0.9$). The presented fully-developed flow rates (F) present the maximum possible limiting values which can be physically induced in the free-convection regime under thermal boundary conditions of the fourth kind. The results show that F increases with both N and E except for small values of N and E in case 4.I. The bulk fluid temperature increases with eccentricity for both cases 4.I and 4.O for all radius ratio except for case 4.I with small radius ratio where it decreases with the eccentricity E. Both the flow rate F and the heat absorbed Q in case 4.O is larger, for given N and E, than the corresponding values in case 4.I. This is a result of the larger heating surface in the former case than the latter.

References

Abdulhadi, J. and Chato, J.C. (1977), "Combined natural and forced convective cooling of underground electric cables", *IEEE Transactions on Power Apparatus and Systems*, Vol. 96, pp. 1-8.

Cheng, K.C. and Hwang, G.J. (1968), "Laminar forced convection in eccentric annuli", *A.I.Ch.E. Journal*, Vol. 14 No. 3, pp. 510-12.

Cladwell, J. (1930), "The hydraulic mean depth as a basis for form comparison in the flow of fluids in pipes", *J.R. Tech. Coll (Glasgow)*, Vol. 2, pp. 203-20.

El-Saden, M.R. (1961), "Heat conduction in an eccentrically hollow, infinitely long cylinder with internal heat generation", *ASME Transactions, Journal of Heat Transfer*, Vol. 83 No. 4, pp. 510-11.

El-Shaarawi, M.A.I. and Al-Nimr, M.A. (1990), "Fully developed natural convection in open-ended vertical concentric annuli", *International Journal of Heat and Mass Transfer*, Vol. 33 No. 9, pp. 1873-84.

El-Shaarawi, M.A.I. and Mokheimer, I. (1995), "Unsteady conduction in eccentric annuli", *Heat and Mass Transfer (Warme- und Stoffubertragung)*, Vol. 30, pp. 249-57.

El-Shaarawi, M.A.I. and Mokheimer, E.M.A. (1999), "Developing free convection in open-ended vertical eccentric annuli with isothermal boundaries", *ASME Transactions, Journal of Heat Transfer*, Vol. 121, pp. 63-72.

El-Shaarawi, M.A.I., Mokheimer, E.M.A. and Abualhamayel, H.I. (2001), "Limiting values for free-convection induced flow rates in vertical eccentric annuli with an isothermal boundary", *Numerical Heat Transfer, Part A*, Vol. 39 No. 6, pp. 611-30.

Feldman, E.E., Hornbeck, R.W. and Osterle, J.F. (1982a), "A numerical solution of laminar developing flow in eccentric annular ducts", *International Journal of Heat and Mass Transfer*, Vol. 25 No. 2, pp. 231-41.

Feldman, E.E., Hornbeck, R.W. and Osterle, J.F. (1982b), "A numerical solution of temperature for laminar developing flow in eccentric annular ducts", *International Journal of Heat and Mass Transfer*, Vol. 25 No. 2, pp. 243-53.

Guckes, T.L. (1975), "Laminar flow of non-newtonian fluids in an eccentric annulus", *ASME Transactions, Journal of Engineering for Industry*, Vol. 97, pp. 498-506.

Heyda, J.F. (1959), "A Green's function solution for the case of laminar incompressible flow between non-concentric cylinders", *J. Franklin Inst.*, Vol. 267, pp. 25-34.

Lowry, W.E., Davis, B.W. and Cheung, H. (1980), "The effect of annular air gaps surrounding an emplaced nuclear waste canister in deep geologic storage", in Kulaki, F.A. and Lyezkowski, R.W. (Eds), *Heat transfer in Nuclear Waste Disposal*, ASME Winter Annual Meeting HTD, pp. 1169-76.

Notaro, R.S. and Webster, D.J. (1971), "Thermal analysis of forced cooled cables", *IEEE Transactions on Power Apparatus and Systems*, Vol. 90, pp. 1225-31.

Piercy, N.A.V., Hooper, M.S. and Winny, H.F. (1933), "Viscous flow through pipes with cores", *London, Edinburgh, Dublin, Philos. Mag. J. Sci*, Vol. 15, pp. 647-76.

Redberger, P.J. and Charles, M.E. (1962), "Axial laminar flow in a circular pipe containing a fixed eccentric core", *The Canadian Journal of Chemical Engineering*, pp. 148-51.

Reynolds, W.C., Lundberg, R.E. and McCuen, P.A. (1963), "Heat transfer in annular passages. General formulation of the problem for arbitrarily prescribed wall temperatures or heat fluxes", *International Journal of Heat and Mass Transfer*, Vol. 6, pp. 483-93.

Snyder, W.T. (1963), "An analysis of slug flow heat transfer in an eccentric annulus", *A.I.Ch.E. Journal*, Vol. 9 No. 4, pp. 503-6.

Snyder, W.T. and Goldstein, G.A. (1965), "An analysis of a fully developed laminar flow in an eccentric annulus", *A.I.Ch.E. Journal*, Vol. 11 No. 3, pp. 462-9.

Trombeta, M.L. (1972), "Laminar forced convection in eccentric annuli", *International Journal of Heat and Mass Transfer*, Vol. 14, pp. 1161-72.

Yonggang, Z. and Junfang, H. (1995), "Study of the displacement mechanics for non-newtonian fluid and its application in well cementing techniques", *Journal of Hydrodynamics*, Vol. 7 No. 3, pp. 107-10.